

1 **Atmospheric mercury in the southern hemisphere – Part 1: Trend and inter-**  
2 **annual variations of atmospheric mercury at Cape Point, South Africa, in 2007**  
3 **-2017, and on Amsterdam Island in 2012 - 2017**

5 Franz Slemr<sup>1</sup>, Lynwill Martin<sup>2</sup>, Casper Labuschagne<sup>2</sup>, Thumeka Mkoikolo<sup>2</sup>, H el ene Angot<sup>3</sup>,  
6 Olivier Magand<sup>4</sup>, Aur elien Dommergue<sup>4</sup>, Philippe Garat<sup>5</sup>, Michel Ramonet<sup>6</sup>, Johannes Bieser<sup>7</sup>

8 Corresponding author: [Franz.Slemr@mpic.de](mailto:Franz.Slemr@mpic.de)

9 Second corresponding author: [Lynwill.Martin@weathersa.co.za](mailto:Lynwill.Martin@weathersa.co.za)

Feldfunktion ge ndert

12 <sup>1</sup>Max-Planck-Institut f ur Chemie (MPI), Air Chemistry Division, Hahn-Meitner-Weg 1, D-55128 Mainz,  
13 Germany

14 <sup>2</sup>South African Weather Service c/o CSIR, P.O.Box 320, Stellenbosch 7599, South Africa

15 <sup>3</sup>Institute of Arctic and Alpine Research, University of Colorado Boulder, Boulder, CO, USA

16 <sup>4</sup>Institut des G eosciences de l'Environnement, Univ Grenoble Alpes, CNRS, IRD, Grenoble INP, 38400  
17 Grenoble, France

18 <sup>5</sup>LJK, Univ Grenoble Alpes, CNRS, IRD, Grenoble INP, 38401 Grenoble, France

19 <sup>6</sup>Laboratoire des Sciences du Climat et de l'Environnement, LSCE-IPSL (CEA-CNRS-UVSQ), Universit e  
20 Paris-Saclay, 91191 Gif-sur-Yvette, France

21 <sup>7</sup>Helmholtz-Zentrum Geesthacht (HZG), Institute of Coastal Research, Max-Planck-Str. 1, D-21502  
22 Geesthacht, Germany

27 **Abstract**

28 The Minamata Convention on mercury (Hg) entered into force in 2017, committing its 116 parties (as  
29 of January 2019) to curb anthropogenic emissions. Monitoring of atmospheric concentrations and  
30 trends is an important part of the effectiveness evaluation of the Convention. A few years ago (in 2017)  
31 we reported an increasing trend of atmospheric Hg concentrations at the Cape Point Global  
32 Atmospheric Watch (GAW) station in South Africa (34 21'S, 18 29'E) for the 2007 – 2015 period. With

33 2 more years of measurements at Cape Point and the 2012 – 2017 data from Amsterdam Island  
34 (37°48'S, 77°34'E) in the remote southern Indian Ocean, a more complex picture emerges: at Cape  
35 Point the upward trend for the 2007 – 2017 period is still significant but none or slightly downward  
36 trend was detected for the period 2012 – 2017 both at Cape Point and Amsterdam Island. The upward  
37 trend at Cape Point is ~~thus~~-driven mainly by the [Hg concentration minimum in 2009 and maxima in](#)  
38 [2014 and 2012](#)~~2007 – 2014 data~~. Using ancillary data on <sup>222</sup>Rn, CO, O<sub>3</sub>, CO<sub>2</sub>, and CH<sub>4</sub> from Cape Point  
39 and Amsterdam Island the possible reasons for the trend and its change are investigated. In a  
40 companion paper this analysis is extended for the Cape Point station by calculations of source and sink  
41 regions using backward trajectory analysis.

## 42 1 Introduction

43 Mercury (Hg) is an environmental toxicant emitted by both natural and anthropogenic sources – the  
44 latter regulated by the Minamata Convention. This Convention, which entered into force in August  
45 2017, requires periodic effectiveness evaluation (Article 22) to ensure that it meets its objectives. This  
46 evaluation will be based on a combination of Hg monitoring data, including levels of Hg and Hg  
47 compounds in air, biota, and humans. A few years ago, we reported an upward trend of atmospheric  
48 mercury concentrations at the Cape Point Global Atmospheric Watch (GAW) station at Cape Point  
49 (CPT, 34°21'S, 18°29'E) in South Africa for the 2007 – 2015 period (Martin et al., 2017). An upward  
50 trend was surprising because manual mercury measurements at the same site in 1995 – 2004 showed  
51 a downward trend. Downward trends of atmospheric mercury concentrations and of mercury wet  
52 deposition have also been reported for many sites in the northern hemisphere (Temme et al., 2007;  
53 Cole et al., 2014; Steffen et al., 2015; Weigelt et al., 2015; Weiss-Penzias et al., 2016; Marumoto et al.,  
54 2019) but Cape Point has been the only station in the southern hemisphere with a long enough  
55 mercury concentration record to calculate trends. The northern hemispheric downward trend has  
56 been attributed to decreasing emissions from the North Atlantic Ocean due to decreasing mercury  
57 concentrations in subsurface water (Soerensen et al., 2012) and more recently to decreasing global  
58 anthropogenic emissions mainly due to the decline of mercury release from commercial products and  
59 the changes of Hg<sup>0</sup>/Hg<sup>2+</sup> speciation in flue gas of coal-fired utilities after implementation of NO<sub>x</sub> and  
60 SO<sub>2</sub> emission controls (Zhang et al., 2016). Mercury uptake by terrestrial vegetation has also been  
61 recently proposed to contribute to the downward trend (Jiskra et al., 2018).

62 In the meantime, mercury measurements at several other sites in the southern hemisphere have  
63 become available (Sprovieri et al., 2016, 2017). Atmospheric mercury is quite uniformly distributed  
64 throughout the southern hemisphere (Slemr et al., 2015) and its concentrations (~ 1.0 ng m<sup>-3</sup>) are  
65 substantially lower than those found at remote sites in the northern hemisphere (~1.45 ng m<sup>-3</sup>)  
66 (Sprovieri et al., 2016). Opposite to a pronounced seasonal variation with a maximum in early spring

67 and a minimum in autumn in the northern hemisphere (Sprovieri et al., 2016), hardly any seasonal  
68 variation has been observed at Cape Point and Amsterdam Island (Slemr et al., 2015). The absence of  
69 a pronounced seasonal variation in the southern hemisphere has been recently attributed to mercury  
70 uptake by the terrestrial vegetation which, due to land distribution, is smaller in the southern  
71 hemisphere (Jiskra et al., 2018).

72 In this paper we analyse the Cape Point (CPT) data for the 2007-2017 period and compare them with  
73 the data from Amsterdam Island (AMS) obtained in the years 2012-2017. Mercury concentrations  
74 remains nearly constant at both sites during the 2012 – 2017 period. Using simultaneously measured  
75  $^{222}\text{Rn}$ ,  $\text{CO}$ ,  $\text{O}_3$ ,  $\text{CO}_2$ , and  $\text{CH}_4$  concentrations at CPT and AMS we investigate the possible reasons for the  
76 trend and its change.

## 77 2 Experimental

78 The locations of the Cape Point (CPT) and Amsterdam Island (AMS) stations are shown in Figure 1. The  
79 Cape Point station (CPT, 34°21'S, 18°29'E) is located on the southern tip of the Cape Peninsula within  
80 the Cape Point National Park at the summit of a 230 m a.s.l. peak about 60 km south of Cape Town.  
81 The site is operated as one of the Global Atmospheric Watch (GAW) baseline monitoring observatories  
82 of the World Meteorological Organisation (WMO) by South African Weather Service and its current  
83 continuous measurements include Hg, CO, O<sub>3</sub>, CH<sub>4</sub>, CO<sub>2</sub>,  $^{222}\text{Rn}$ , N<sub>2</sub>O, several halocarbons, particles, and  
84 meteorological parameters (Martin et al., 2017).

85 Amsterdam Island (AMS, 37°48'S, 77°34'E) is a small island (55 km<sup>2</sup>) in the southern Indian Ocean,  
86 3400 km and 5000 km downwind of Madagascar and South Africa, respectively. The station is located  
87 at Pointe Bénédicte, at the northwest end of the island at an altitude of 55m a.s.l. Labelled GAW/WMO  
88 Global site, the Amsterdam site hosts instruments occurring in the framework of the French national  
89 observation service named ICOS-France-Atmosphere as well as the Global Observation System for  
90 Mercury (GOS4M), for long-term monitoring of greenhouse gases and mercury species, respectively.  
91 The site is ensured by the administration of Terres Australes and Antarctiques Françaises (TAAF), the  
92 French Southern and Antarctic Lands, and scientifically operated by the French Polar Institute (IPEV).  
93 Currently, CO, O<sub>3</sub>, CO<sub>2</sub>, CH<sub>4</sub>,  $^{222}\text{Rn}$ , total aerosol number, carbonaceous aerosol, and meteorological  
94 parameters are continuously monitored at the site (Angot et al., 2014).

95 Atmospheric mercury has been measured since March 2007 at CPT and since January 2012 at AMS  
96 using Tekran 2537 (Tekran Inc., Toronto, Canada) at both sites. The instruments are based on mercury  
97 enrichment on a gold cartridge, followed by a thermal desorption and a detection by cold vapour  
98 atomic fluorescence spectroscopy (CVAFS). Switching between two cartridges allows for alternating  
99 sampling and desorption and thus results in a full temporal coverage of the mercury measurement.

Feldfunktion geändert

100 The instruments are automatically calibrated every 25 h at CPT and every 69 h at AMS using internal  
101 mercury permeation sources which in turn were annually checked by manual injections of saturated  
102 Hg vapour from a temperature-controlled vessel. To ensure the comparability of the mercury  
103 measurements, Tekran instruments at both sites have been operated according to the Global Mercury  
104 Observation System (GMOS) standard operating procedures (SOP, Munthe et al., 2011).

105 The instrument at CPT has been operated with 15 min resolution since March 2007. At AMS, the Tekran  
106 speciation unit (Tekran 1130 and 1135) coupled to the Tekran 2537B analyser (Tekran Inc. Toronto,  
107 Canada) was in operation since January 2012 until December 10, 2015. Gaseous elemental mercury  
108 (GEM) was measured with 5 min resolution during this period. Concentrations of gaseous oxidized  
109 (GOM) and particulate mercury (PM) were below the detection limit for most of the time (Angot et al.,  
110 2014). Consequently, only GEM has been continuously measured with Tekran 2537A/B analyser since  
111 December 14, 2015, with a resolution of 15 min as at the Cape Point while GOM and PM species  
112 continued to be collected on CEM filters on weekly frequencies.

113 With GEM concentrations of  $\sim 1 \text{ ng m}^{-3}$  and a sampling flow rate of  $1 \text{ l (STP) min}^{-1}$  mercury loads on gold  
114 cartridges are  $\sim 5 \text{ pg}$  and  $\sim 15 \text{ pg}$  with 5 min and 15 min long sampling, respectively. A measurement  
115 bias with loads  $< 10 \text{ ng m}^{-3}$  due to internal Tekran integration procedure (Swartzendruber et al., 2009;  
116 Slemr et al., 2016a; Ambrose, 2017) can impair comparability of the measurements made with 5 min  
117 resolution with those made with 15 min resolution. The possible bias of the measurements at AMS in  
118 2012-2015 was eliminated by optimising the integration parameters (Swartzendruber et al., 2009). The  
119 absence of bias was shown by calculating the monthly variation coefficients of the 5 and the 15 min  
120 measurements at AMS. The average monthly variation coefficients were  $5.81 \pm 2.15 \%$  ( $n=48$ ) and  $5.83$   
121  $\pm 1.48 \%$  ( $n=24$ ) for 5 min and 15 min resolution, respectively, and they are statistically not  
122 distinguishable. We thus conclude that the measurements at AMS with 5 min resolution are  
123 comparable to those with 15 min.

### 124 **3 Results and discussion**

#### 125 3.1 Seasonal variation

126 Figure 24 shows seasonal GEM variations at CPT (upper panel) and AMS (lower panel). They were  
127 calculated by averaging of monthly medians over the period of 2012 – 2017. Similar plots were  
128 obtained by averaging of monthly averages in the same period. The amplitude of the seasonal variation  
129 at AMS is with  $> 0.1 \text{ ng m}^{-3}$  somewhat larger than at CPT ( $\sim 0.08 \text{ ng m}^{-3}$ ). The standard deviations of  
130 monthly average concentrations are larger at CPT than at AMS indicating higher interannual variation  
131 at CPT. Smaller standard deviations at AMS enable to detect significant differences between the  
132 months with the highest (June, July, and August) and the lowest three (November, February, and

133 October) GEM concentrations. GEM concentrations in December and January lie outside of an  
134 otherwise nearly sinusoidal seasonal variation but their differences to GEM averages in other months  
135 are not significant. No significant differences between monthly averages at CPT were found.

136 In summary, maximum GEM concentrations at AMS are observed in austral winter (June – August) and  
137 the lowest GEM concentrations in austral summer. Austral winter is the season with the most frequent  
138 fast transport from southern Africa to AMS (June – October; Miller et al., 1993) coinciding also with  
139 maximum <sup>222</sup>Rn concentrations at AMS (May – August) as another indicator of continental influence  
140 (Polian et al., 1986). The most frequent events at AMS in 1996 – 1997 with high CO mixing ratios  
141 occurred also in austral winter (June – October, Gros et al., 1999). Biomass burning in southern Africa  
142 peaks in austral winter **and spring** (July – October, Duncan et al., 2003) and we therefore conclude, in  
143 agreement with Angot et al. (2014), that mercury from biomass burning in southern Africa combined  
144 with its fast transport to AMS is mostly responsible for the seasonal variation observed there. Reduced  
145 uptake of atmospheric GEM by terrestrial biomass of southern Africa in austral winter (Jiskra et al.,  
146 2018) can also contribute.

### 147 3.2 Trends at CPT in 2007 - 2017

148 Figure 32 shows annual median GEM concentrations at CPT (2007 – 2017) and at AMS (2012 – 2017).  
149 Table 1 shows the trends of GEM, CO<sub>2</sub>, <sup>222</sup>Rn, CO, CH<sub>4</sub>, and O<sub>3</sub> at CPT in the 2007-2017 period as  
150 calculated by least square fit of monthly averages or medians (medians are shown in Figure 1 of  
151 Supporting Information). Monthly average and median GEM concentrations show a significant upward  
152 trend of  $7.69 \pm 2.11$  and  $7.01 \pm 2.11$  pg m<sup>-3</sup> yr<sup>-1</sup>, respectively. The upward trends of CO<sub>2</sub> ( $2.07 \pm 0.03$   
153 ppm yr<sup>-1</sup> for averages and  $2.08 \pm 0.02$  ppm yr<sup>-1</sup> for medians) and CH<sub>4</sub> ( $5.70 \pm 0.66$  ppb yr<sup>-1</sup> for averages  
154 and  $5.85 \pm 0.53$  ppb yr<sup>-1</sup> for medians) are comparable to worldwide trends of 2.24 ppm yr<sup>-1</sup> for CO<sub>2</sub> and  
155 6.9 ppb yr<sup>-1</sup> for CH<sub>4</sub> in 2008-2017 (WMO Greenhouse Gas Bulletin, 2018) . For the interpretation of the  
156 GEM trend, the most revealing is the non-significant trend in <sup>222</sup>Rn and the significant downward trend  
157 in CO. <sup>222</sup>Rn is a radioactive gas of predominantly terrestrial origin with a half-life of 3.8 days. Non-  
158 significant <sup>222</sup>Rn trend thus implies a nearly constant ratio of oceanic to continental air masses over  
159 the 2007 – 2017 period and rules out larger shifts in climatology of CPT as the cause of the observed  
160 GEM trend. Biomass burning is a major source of CO in the southern hemisphere (Duncan et al., 2003;  
161 Pirrone et al., 2010) and at the same time a major source of Hg (Friedli et al., 2009). The downward  
162 trend of CO thus rules out increasing Hg emissions from biomass burning to be responsible for the  
163 upward GEM trend at CPT. The downward trend of CO at CPT is consistent with the decreasing CO  
164 emissions in 2001 – 2015 (Jiang et al., 2017). They report decreasing CO emissions from biomass  
165 burning from boreal North America, boreal Asia and South America **but** no change in Africa.

166 3.3 Trends at CPT and AMS in 2012 - 2017

167 Monthly GEM averages and medians at AMS and CPT in the 2012 - 2017 period are not statistically  
168 distinguishable according to the paired student t test. Monthly CO<sub>2</sub> averages at CPT are significantly  
169 higher than at AMS (at >99.9% significance level) but medians cannot be distinguished. Medians of  
170 CO<sub>2</sub>, <sup>222</sup>Rn, CO, and CH<sub>4</sub> are less influenced by occasional events with extremely high values and as such  
171 tend to be smaller than averages. Because such events are less frequent at AMS than at CPT, the  
172 differences between monthly averages and medians are always higher at CPT than at AMS. This  
173 explains why the CO<sub>2</sub> monthly averages are significantly higher at CPT than at AMS but the medians  
174 are not. Similarly, the significance of the monthly differences between higher CO at CPT and lower at  
175 AMS is >99.9% for averages but only >99% for medians. Monthly CH<sub>4</sub> mixing ratios are always higher  
176 at CPT than at AMS with >99.9% significance both for averages and medians. The most pronounced  
177 difference between CPT and AMS is in <sup>222</sup>Rn concentrations: monthly averages and medians at CPT are  
178 on average 16.6 and 12.6 times higher, respectively, than at AMS. In summary, higher monthly CO<sub>2</sub>,  
179 CO, CH<sub>4</sub>, and especially <sup>222</sup>Rn averages and medians at CPT than at AMS clearly demonstrate higher  
180 influence of continental air masses at CPT because all these species are predominantly of terrestrial  
181 origin. Statistically comparable GEM concentrations at AMS and CPT in 2012 – 2017, on the contrary,  
182 suggest that terrestrial GEM sources do not play a major role and oceanic sources are dominating at  
183 CPT. This conclusion is supported by an analysis of GEM/<sup>222</sup>Rn ratios in events with enhanced <sup>222</sup>Rn  
184 concentrations observed at CPT (Slemr et al., 2013) which found terrestrial surface of southern Africa  
185 to be rather a sink of GEM than a source. This is further discussed in the companion paper (Bieser et  
186 al., 2019).

187 Tables 2 and 3 shows the 2012 – 2017 trends of GEM, CO<sub>2</sub>, <sup>222</sup>Rn, CO, and CH<sub>4</sub> at AMS and CPT,  
188 respectively. The AMS monthly average and median GEM concentrations do not show any significant  
189 trend. At CPT monthly average GEM concentrations do not show any significant trend, whereas median  
190 GEM concentrations show a significant slight downward trend (at >95% significance level). As in the  
191 2007-2017 period the neutral to slightly downward GEM trend at CPT is accompanied by no significant  
192 trend in <sup>222</sup>Rn. Opposite to the 2007 – 2017 period CO does not show any significant downward trend  
193 whereas O<sub>3</sub> (not listed) shows a small significant upward trend in monthly averages but not in monthly  
194 medians.

195 An inspection of Figure 32 shows that the GEM trend at CPT in 2007 – 2017 period is driven mainly by  
196 the minimum in 2009 and the maxima in 2012 and –2014-period. Table 1 of supporting information  
197 (SI) shows the trends of GEM, <sup>222</sup>Rn, CO, CH<sub>4</sub>, and O<sub>3</sub> at CPT for the 2007 – 2014 period. Monthly  
198 average and median GEM concentrations increased by  $16.91 \pm 3.60$  and  $16.18 \pm 3.61$  pg m<sup>-3</sup> yr<sup>-1</sup>,

199 respectively. This upward GEM trend is accompanied by no trend in <sup>222</sup>Rn and O<sub>3</sub>, and small downward  
200 trend in monthly average CO mixing ratios but not in medians.

201 In summary, the 2007 – 2017 time series of GEM concentrations at CPT consists of two parts: one  
202 starting in 2007 and ending approximately in 2014 with a pronounced upward trend and the other  
203 without any [\(medians and averages at AMS and averages at CPT\)](#) or even slightly downward trend  
204 [\(medians at CPT\)](#) starting in 2012. The absence of GEM trend [in averages](#) in 2012 – 2017 at CPT is in  
205 agreement with the absence of the GEM trend at AMS in the same period. The upward trend thus  
206 appears to have changed between 2012 and 2014. The absence of <sup>222</sup>Rn trends at CPT for 2007 – 2017  
207 and the subperiods 2007 – 2014 and 2012 - 2017 points to nearly constant ratio of marine and  
208 continental air masses over the years and thus rules out shifts in regional climatology being responsible  
209 for the GEM trends. A downward trend of CO over the 2007 – 2017 period and none or just significantly  
210 downward one for the subperiods 2007 – 2014 and 2012 – 2017 makes it unlikely that increasing Hg  
211 emissions from biomass burning could be the reason for upward trend of GEM concentrations at CPT.  
212 We note that both <sup>222</sup>Rn concentrations and CO mixing ratios have a very pronounced seasonal  
213 variations which make it difficult to determine significant trends over shorter periods.

#### 214 3.4 Inter-annual variations of GEM concentrations

215 A plot of annual median GEM concentrations in Figure [32](#) (annual averages provide a very similar  
216 pattern and are not shown) shows that median concentrations in 2007 and 2008 are only slightly lower  
217 than in 2015 - 2017. It is the steady increase from the lowest GEM concentrations in 2009 to the highest  
218 ones in 2014 at CPT (the latter 2<sup>nd</sup> highest at AMS in 2012 – 2017 period) which seems to be responsible  
219 for the upward trend in 2007 – 2017 at CPT and no trend for 2012 -2017 period for both CPT and AMS.  
220 Exceptionally low annual GEM concentrations in 2009 (average and median of 0.918 and 0.913 ng m<sup>-3</sup>,  
221 <sup>3</sup>, respectively) and exceptionally high ones in 2014 (average and median of 1.090 and 1.094 ng m<sup>-3</sup>,  
222 respectively, at CPT, 1.050 and 1.053 ng m<sup>-3</sup>, respectively, at AMS) seem to be a near global  
223 phenomenon. The years 2009 and 2014 show the largest deviations (a negative one in 2009, a positive  
224 one in 2014) from the linear 2000 - 2014 trend of annual GEM average concentrations recorded at 18  
225 sites in North America (Figure 8 b of Streets et al., 2019). At Mace Head, a site in Ireland, GEM annual  
226 average and median concentrations in 2009 were the lowest over the 1996 – 2013 period (supporting  
227 Information of Weigelt et al., 2015). The reasons for these near global inter-annual variations are not  
228 clear. Global anthropogenic Hg emissions do not vary much from year to year (mostly by less than 5%)  
229 and have been steadily increasing over the 2010 – 2015 period (Streets et al., 2019). Between 2000  
230 and 2010 they steadily increased by ~10% (Streets et al., 2017 and 2019). These emission estimates do  
231 not include Hg from biomass burning but CO emissions from biomass burning, as a proxy for Hg  
232 emissions, were somewhat lower in 2008 and 2009 but not exceptionally high in 2014 (Jiang et al.,

233 2017). Annual volcanic SO<sub>2</sub> emissions, as a proxy for volcanic Hg emissions, also do not show  
234 exceptionally low emissions in 2009, although the emissions in 2014 were the second highest (after  
235 2011) on record in the 1996 – 2018 period ([https://disc.gsfc.nasa.gov/datasets/MSVOLSO2L4\\_V-](https://disc.gsfc.nasa.gov/datasets/MSVOLSO2L4_V-3/summary)  
236 [3/summary](https://disc.gsfc.nasa.gov/datasets/MSVOLSO2L4_V-3/summary)).

Feldfunktion geändert

237 Tropospheric mercury concentrations were found to be influenced by El Niño Southern Oscillation  
238 (ENSO) (Slemr et al., 2016b). Such influence could also be a reason for the observed inter-annual  
239 variation of GEM concentrations at Cape Point. Table 4 shows correlations of 3 months running  
240 averages and medians of GEM concentration at CPT with 3 months running average of Southern  
241 Oscillation Index (SOI) for 2007 – 2014 and 2012 – 2017 and compares them with the 2012 – 2017  
242 period at AMS. 3 month running averages and medians were taken instead of monthly averages to  
243 take account for time of intra-hemispheric mixing. Correlations of CO mixing ratios with SOI  
244 ([www.cpc.ncep.noaa.gov/data/indices/soi.3m.txt](http://www.cpc.ncep.noaa.gov/data/indices/soi.3m.txt)) at CPT for 2007 – 2014 and 2012 – 2017 are also  
245 listed. CO vs SOI correlations for AMS were not made because the CO mixing ratios are available only  
246 since December 2015 until December 2017.

Feldfunktion geändert

247  
248 Table 4 shows ~~inverse~~~~negative~~ correlations of GEM concentrations with SOI at AMS for 2012 - 2017  
249 with a lag of 6-8 months both for averages and medians. Relative GEM (after detrending) at CPT also  
250 ~~antic~~correlates ~~inversely~~ with SOI at CPT in the 2007 – 2014 period as does CO mixing ratio  
251 (deseasonalised) in the same period, both with a slightly longer lag of 9 – 11 months. ~~Inverse~~  
252 ~~Anti~~correlations of GEM concentrations and CO mixing ratios with SOI with similar lags were reported  
253 by Slemr et al. (2016b) who interpreted them as a sign for biomass burning being the driving force for  
254 the inter-annual variation of GEM and CO. The ~~correlations of~~ GEM and CO ~~with~~vs SOI ~~correlations~~ for  
255 the 2012 – 2017 period at CPT are both positive and the CO vs SOI correlation is significant only at  
256 >95% level. For the 2007 – 2017 period at CPT, encompassing both periods, ~~also an inverse-negative~~  
257 correlation of GEM vs SOI was found but with a lower significance level of only >95%. The different  
258 correlations of GEM and CO with SOI at CPT for the period 2012 – 2017 from those at CPT in 2007 –  
259 2014 and of GEM vs SOI at AMS in 2012 – 2017 clearly shows that at least at CPT the mechanism for  
260 inter-annual variations changed.

261 Correlations of detrended monthly GEM averages and medians at CPT with North Atlantic Oscillation  
262 (NAO) index  
263 ([www.cpc.ncep.noaa.gov/products/precip/Cwlink/pna/norm.nao.monthly.b5001.current.ascii.table](http://www.cpc.ncep.noaa.gov/products/precip/Cwlink/pna/norm.nao.monthly.b5001.current.ascii.table))  
264 over the period 2007 – 2017 were not significant for medians and just significant (>95%) for averages  
265 with a lag of 11 months. In the 2012 – 2017 period the correlations of GEM with NAO index were  
266 significant (>95%) with a delay of 0- and 8-months both for monthly medians and averages (both not

Feldfunktion geändert



267 detrended). The correlation with 0 months delay is ~~inversenegative~~ and that with 8-month delay is  
268 positive. At AMS monthly GEM averages correlate with NAO index with a delay of 3, 5, and 6 months,  
269 all at a significance level of >95%. Monthly medians correlate with a delay of 5 and 6 months, the latter  
270 even at a significance level of > 99%. In summary, there seems to be some influence of NAO on GEM  
271 concentration. The influence is more pronounced at AMS than at CPT, probably because of more  
272 regional influence at the latter site.

273 The annual GEM minimum in 2009 and the maxima in 201~~2~~<sup>4</sup> and 201~~4~~<sup>2</sup> at CPT as well as the annual  
274 minima in 2015 and 2017 ~~and~~ maxima in 2014 and 2016 at AMS fit a biennial tendency already  
275 mentioned by Martin et al. (2017) with mostly lower annual GEM concentrations in odd years and  
276 higher ones in even years. The biennial tendency is also apparent in the annual median and average  
277 CO mixing ratios at CPT (there are only two years with CO measurements at AMS), with mostly lower  
278 values in odd years and higher ones in even years, similar to GEM concentrations. Meehl and Arblaster  
279 (2001, 2002) note a relation between Tropospheric Biennial Oscillation (TBO) and ENSO, the latter also  
280 with a biennial tendency.

281 In summary, a part of the inter-annual variation of GEM concentrations seems to be related to  
282 teleconnections like ENSO, TBO and NAO.

### 283 **Conclusions**

284 Martin et al. (2017) reported an upward trend of GEM concentrations at CPT from March 2007 to June  
285 2015. With two and a half year of more measurements at CPT until December 2017 and GEM  
286 measurements at AMS since February 2012 until December 2017 a more complex picture emerged:

287 No significant trend of GEM concentrations was found at CPT and AMS for the period of AMS  
288 measurements, i.e. 2012 – 2017. Upward trend of GEM concentrations at CPT in 2007 – 2015 reported  
289 by Martin et al. (2017) is driven mainly by the 2009 – 2014 data with a minimum in 2009 and maxima  
290 in 2012 and 2014. The latter two years with high annual GEM concentrations seem to be the reason  
291 for absent trend in 2012 – 2017 period, although the upward trend over the whole 2007 – 2017 period  
292 at CPT is still significant. A minimum of GEM concentrations in 2009 was also reported for stations in  
293 North America and at Mace Head, Ireland. In addition, annual average and median GEM concentrations  
294 at CPT and AMS show a biennial pattern with lower concentrations in odd years and higher ones in  
295 even years. Because of the pronounced inter-annual variations, the calculated GEM trends will depend  
296 on the year when the observations start and end and increasingly so, the shorter the observation  
297 period is.

298 No trend was found in <sup>222</sup>Rn concentrations and a slight downward trend in CO mixing ratios were  
299 found at CPT in 2007 – 2017. Changing ratios of marine and continental air masses at CPT as well as

300 increasing mercury emissions from biomass burning can, therefore, be ruled out as the cause of the  
301 upward GEM trend at CPT.

302 Monthly average GEM concentrations at CPT and AMS in 2012 – 2017 are statistically indistinguishable  
303 while concentrations of species of terrestrial origin such as CO<sub>2</sub>, CH<sub>4</sub>, CO, and especially of <sup>222</sup>Rn clearly  
304 show substantially higher values at CPT in comparison with those at AMS. Comparable GEM  
305 concentrations at CPT and AMS despite much higher influence of terrestrial air masses at CPT thus  
306 indicate that terrestrial GEM sources are of minor importance and the oceanic GEM sources are  
307 dominating at CPT. This major conclusion will be substantiated by a companion paper in which the  
308 GEM concentration will be, with help of backward trajectories, attributed to different source and sink  
309 regions.

#### 310 Data availability

311 Cape Point data are available on the GMOS website at  
312 [http://sdi.iaa.cnr.it/geoint/publicpage/GMOS/gmos\\_historical.zul](http://sdi.iaa.cnr.it/geoint/publicpage/GMOS/gmos_historical.zul). Amsterdam Island GEM data are  
313 freely available in the catalogue section at <https://gmos.aeris-data.fr>. Those used in this article (AMS  
314 site, L2) have the unique identifier bcb74d91-d6ea-4f83-a897-f98f8eccd044c.

#### 315 Author contribution

316 LM, CL, TM, HA, OM, AD, PG, and MR provided the data on which this work is based. FS made the  
317 statistical analysis and prepared the manuscript in collaboration with LM, HA, OM, and JB.

318 *Competing interests.* The authors declare that they have no conflict of interest.

#### 319 Acknowledgments

320 This publication forms part of the output of the Biogeochemistry Research Infrastructure Platform  
321 (BIOGRIP) of the Department of Science and Innovation of South Africa. We thank CPT team for  
322 providing the data on which this paper is based. We also thank Andreas Weigelt and Ralf Ebinghaus  
323 from Helmholtz-Zentrum in Geesthacht who for years supported mercury measurements at CPT and  
324 Ernst-Günther Brunke who was responsible for CPT operation until he retired in 2015. Olivier Magand,  
325 Aurelien Dommergue and H el ene Angot deeply thank all overwintering staff at AMS, French Polar  
326 Institute Paul-Emile Victor (IPEV) staff and scientists who helped with the setup and maintenance of  
327 the experiment at AMS in the framework of GMOStral-1028 IPEV program. Logistical and financial  
328 supports for AMS are provided by IPEV (GMOStral-1028 program) since 2012. Funds obtained through  
329 the European Union 7<sup>th</sup> Framework Programme project Global Mercury Observation System (GMOS –  
330 [www.gmos.eu](http://www.gmos.eu)), Labex OSUG@2020 (ANR10 LABX56) and LEFE CNRS/INSU (Programme SAMOA) also  
331 contributed to this work. We thank also the IPEV RAMCES-416 programme which provided greenhouse

hat formatiert: Schriftart: Kursiv, Unterstrichen

hat formatiert: Schriftart: Kursiv

Feldfunktion ge ndert

hat formatiert: Schriftart: Kursiv, Unterstrichen

hat formatiert: Schriftart: Kursiv

hat formatiert: Schriftart: Kursiv, Unterstrichen

hat formatiert: Hochgestellt

332 [gas and <sup>222</sup>Rn data for AMS. Last but not least we would also like to thank the reviewers for their](#)  
333 [insightful and constructive feedback, which has helped to improve the clarity and utility of the revised](#)  
334 [manuscript.](#)

hat formatiert: Hochgestellt

335

#### 336 References

337 Ambrose, J.L.: Improved methods for signal processing in measurements of mercury by Tekran 2537A  
338 and 2537B instruments, *Atmos. Meas. Tech.*, **10**, 5063-5073, 2017.

339 Angot, H., Barret, M., Magand, O., Ramonet, M., and Dommergue, A.: A 2-year record of atmospheric  
340 mercury species at a background Southern Hemisphere station on Amsterdam Island, *Atmos. Chem.*  
341 *Phys.*, **14**, 11461-11473, 2014.

342 Cole, A.S., Steffen, A., Eckley, C.S., Narayan, J., Pilote, M., Tordon, R., Graydon, J.A., Louis, V.L.St., Xu,  
343 X., and Branfireun, B.A.: A survey of mercury in air and precipitation across Canada: Patterns and  
344 trends, *Atmosphere*, **5**, 635-668, 2014.

345 Duncan, B.N., Martin, R.V., Staudt, A.C., Yevich, R., and Logan, J.A.: Interannual and seasonal variability  
346 of biomass burning emissions constrained by satellite observations, *J. Geophys. Res.*, **108**, D2, 4100,  
347 doi:10.1029/2002JD002378, 2003.

348 Friedli, H.R., Arellano, A.F., Cinnirella, S., and Pirrone, N.: Initial estimates of mercury emissions to the  
349 atmosphere from global biomass burning, *Environ. Sci. Technol.*, **43**, 3507-3513, 2009.

350 Jiang, Z., Worden, J.R., Worden, H., Deeter, M., Jones, D.B.A., Arellano, A.F., and Henze, D.K.: A 15-year  
351 record of CO emissions constrained by MOPITT CO observations, *Atmos. Chem. Phys.*, **17**, 4565-4583,  
352 2017.

353 Jiskra, M., Sonke, J.E., Obrist, D., Bieser, J., Ebinghaus, R., Lund Myhre, C., Pfaffhuber, K.A., Wängberg,  
354 I., Kyllönen, K., Worthy, D., Martin, L.G., Labuschagne, C., Mkololo, T., Ramonet, M., Magand, O., and  
355 Dommergue, A.: A vegetation control on seasonal variations in global atmospheric mercury  
356 concentrations, *Nature Geosci.*, **11**, 244-250, 2018.

357 Gros, V., Bonsang, B., Martin, D., Novelli, P.C., and Kazan, V.: Carbon monoxide short term  
358 measurements at Amsterdam Island: estimation of biomass burning emission rates, *Chemosphere*  
359 *Global Change Sci.*, **1**, 163-172, 1999.

360 Jiang, Z., Worden, J.R., Worden, H., Deeter, M., Jones, D.B.A., Arellano, A.F., and Henze, D.K.: A 15-year  
361 record of CO emission constrained by MOPITT CO observations, *Atmos. Chem. Phys.*, **17**, 4565-4583,  
362 2917.

363 Martin, L.G., Labuschagne, C., Brunke, E.-G., Weigelt, A., Ebinghaus, R., and Slemr, F.: Trend of  
364 atmospheric mercury concentrations at Cape Point for 1995-2004 and since 2007, *Atmos. Chem. Phys.*,  
365 17, 2393-2399, 2017.

366 Marumoto, K., Suzuki, N., Shibata, Y., Takeuchi, A., Takami, A., Fukuzaki, N., Kawamoto, K., Mizohata,  
367 A., Kato, S., Yamamoto, T., Chen, J., Hattori, T., Nagasaka, H., and Saito, M.: Long-term observation of  
368 atmospheric speciated mercury during 2007 – 2018 at Cape Hedo, Okinawa, Japan, *Atmosphere*, 10,  
369 362, doi:10.3390/atmos10070362, 2019.

370 Meehl, G.A., and Arblaster, J.M.: The tropospheric biennial oscillation and Indian monsoon rainfall,  
371 *Geophys. Res. Lett.*, 28, 1731-1734, 2001.

372 Meehl, G.A., and Arblaster, J.M.: The tropospheric biennial oscillation and Asian – Australian monsoon  
373 rainfall, *J. Climate*, 15, 722-743, 2002.

374 Miller, J.M., Moody, J.L., Harris, J.M., and Gaudry, A.: A 10-year trajectory flow climatology for  
375 Amsterdam Island, 1980-1989, *Atmos. Environ.*, 27A, 1909-1916, 1993.

376 Munthe, J., Sprovieri, F., Horvat, M., and Ebinghaus, R.: SOPs and QA/QC protocols regarding  
377 measurements of TGM, GEM, RGM, TPM and mercury in precipitation in cooperation with WP3, WP4,  
378 and WP5, GMOS deliverable 6.1, CNR-IA, IVL, available at <http://www.gmos.eu> (last access on ), 2011.

379 Pirrone, N., Cinnirella, S., Feng, X., Finkelman, S.B., Friedli, H.R., Leaner, J., Mason, R., Mukherjee, A.B.,  
380 Stracher, G.B., Streets, D.G., and Telmer, K.: Global mercury emissions to the atmosphere from  
381 anthropogenic and natural sources, *Atmos. Chem. Phys.*, 10, 5951-5964, 2010.

382 Polian, G., Lambert, G., Ardouine, B., and Jegou, A.: Long-range transport of continental radon in  
383 subantarctic and antarctic areas, *Tellus*, 38B, 178-189, 1986.

384 Slemr, F., Brunke, E.-G., Whittlestone, S., Zahorowski, W., Ebinghaus, R., Kock, H.H., and Labuschagne,  
385 C.: <sup>222</sup>Rn-calibrated mercury fluxes from terrestrial surface of southern Africa, *Atmos. Chem. Phys.*, 13,  
386 6421-6428, 2013.

387 Slemr, F., Angot, H., Dommergue, A., Magand, O., Barret, M., Weigelt, A., Ebinghaus, R., Brunke, E.-G.,  
388 Pfaffhuber, K.A., Edwards, G., Howard, D., Powell, J., Keywood, M., and Wang, F.: Comparison of  
389 mercury concentrations measured at several sites in the Southern Hemisphere, *Atmos. Chem. Phys.*  
390 15., 3125-3133, 2015.

391 Slemr, F., Weigelt, A., Ebinghaus, R., Kock, H.H., Bödewadt, J., Brenninkmeijer, C.A.M., Rauthe-Schöch,  
392 A., Weber, S. Hermann, M., Becker, J., Zahn, A., and Martinsson, B.: Atmospheric mercury  
393 measurements onboard CARIBIC passenger aircraft, *Atmos. Meas. Tech.*, 9, 2291-2302, 2016a.

Feldfunktion geändert

394 Slemr, F., Brenninkmeijer, C.A., Rauthe-Schöch, A., Weigelt, A., Ebinghaus, R., Brunke, E.G., Martin, L.,  
395 Spain, T.G., and O ´Doherty, S.: El Niño-Southern Oscillation influence on tropospheric mercury  
396 concentrations, *Geophys. Res. Lett.*, **43**, 1766-1771, 2016b.

397 Soerensen, A.L., Jacob, D.J., Streets, D.G., Witt, M.L.I., Ebinghaus, R., Mason, R.P., Andersson, M., and  
398 Sunderland, E.M.: Multi-decadal decline of mercury in the North Atlantic atmosphere explained by  
399 changing subsurface seawater concentrations, *Geophys. Res. Lett.*, **39**, L21810,  
400 doi:10.1029/2012GL053736, 2012.

401 Sprovieri, F., Pirrone, N., Bencardino, N., D´Amore, F., Carbone, F., Cinnirella, S., Mannarino, V., Landis,  
402 M., Ebinghaus, R., Weigelt, A., Brunke, E.-G., Labuschagne, C., Martin, L., Munthe, J., Wängberg, I.,  
403 Artaxo, P., Morais, F., de Melo Jorge Barbosa, H., Brito, J., Cairns, W., Barbante, C., del Carmen Diéguez,  
404 M., Garcia, P.E., Dommergue, A., Angot, H., Magand, O., Skov, H., Horvat, M., Kotnik, J., Read, K.A.,  
405 Mendes Leves, L., Gawlik, B.M., Sena, F., Mashyanov, N., Obolkin, V., Wip, D., Feng, X.B., Zhang, H., Fu,  
406 X., Ramachandran, R., Cossa, D., Knoery, J., Maruszczak, N., Nerentorp, M., and Norstrom, C.:  
407 Atmospheric mercury concentrations observed at ground-based monitoring sites globally distributed  
408 in the framework of the GMOS network, *Atmos. Chem. Phys.*, **16**, 11915-11935, 2016.

409 Sprovieri, F., Pirrone, N., Bencardino, N., D´Amore, F., Angot, H., Barbante, C., Brunke, E.-G., Arcega-  
410 Cabrera, F., Cairns, W., Comero, S., del Carmen Diéguez, M., Dommergue, A., Ebinghaus, R., Feng, X.B.,  
411 Fu, X., Garcia, P.E., Gawlik, P.M., Hageström, U., Hansson, K., Horvat, M., Kotnik, J., Labuschagne, C.,  
412 Magand, O., Martin, L., Mashyanov, N., Mkololo, T., Munthe, J., Obolkin, V., Ramirez Islas, M., Sena, F.,  
413 Somerset, V., Spandow, P., Vardè, M., Walters, C., Wängberg, I., Weigelt, A., Yang, X., and Zhang, H.:  
414 Five-year records of mercury deposition flux at GMOS sites in the Northern and Southern hemispheres,  
415 *Atmos. Chem. Phys.*, **17**, 2689-2708, 2017.

416 Steffen, A., Lehnerr, I., Cole, A., Ariya, P., Dastoor, A., Durnford, D., Kirk, J., and Pilote, M.:  
417 Atmospheric mercury in the Canadian Arctic. Part I: A review of recent field measurements, *Sci. Tot.*  
418 *Environ.*, 509-510, 3-15, 2015.

419 Streets, D.G., Horowitz, H.M., Jacob, D.J., Lu, Z., Levin, L., ter Schure, A.F.H., and Sunderland, E.M.:  
420 Total mercury released to the environment by human activities, *Environ. Sci. Technol.*, **51**, 5969-5977,  
421 2017.

422 Streets, D.G., Horowitz, H.M., Lu, Z., Levin, L., Thackray, C.P., and Sunderland, E.M.: Global and regional  
423 trends in mercury emissions and concentrations, 2010 – 2015, *Atmos. Environ.*, **201**, 417-2015, 2019.

424 Swartzendruber, P.C., Jaffe, D.A., and Finley, B.: Improved fluorescence peak integration in the Tekran  
425 2537 for applications with sub-optimal sample loadings, *Atmos. Environ.*, **43**, 3648-3651, 2009.

426 Temme, C., Blanchard, P., Steffen A., Banic, C., Beauchamp, S., Poissant, L., Tordon, R., and Wiens, B.:  
427 Trend, seasonal and multivariate analysis study of total gaseous mercury data from the Canadian  
428 atmospheric mercury measurement network (CAMNet), *Atmos. Environ.*, 41, 5423-5441, 2007.

429 Weigelt, A., Ebinghaus, R. Manning, A.J., Derwent, R.G., Simmonds, P.G., Spain, T.G., Jennings, S.G.,  
430 and Slemr, F.: Analysis and interpretation of 18 years of mercury observations since 1996 at Mace  
431 Head, Ireland, *Atmos. Environ.*, 100, 85-93, 2015.

432 Weiss-Penzias, P.S., Gay, D.A., Brigham, M.E., Parsons, M.T., Gustin, M.S., and ter Schure, A.: Trends in  
433 mercury wet deposition and mercury air concentrations across the U.S. and Canada, *Sci. Tot. Environ.*,  
434 568, 546-556, 2016.

435 WMO Greenhouse Gas Bulletin, No. 14, 22 November 2018.

436 Zhang, Y., Jacob, D.J., Horowitz, H.M., Chen, L., Amos, H.M., Krabbenhoft, D.P., Slemr, F., Louis, V.L.St.,  
437 and Sunderland, E.M.: Observed decrease in atmospheric mercury explained by global decline in  
438 anthropogenic emissions, *PNAS*, 113, 526-531, 2016.

439

440

441 **Tables**

442 *Table 1. Trends at Cape Point for the 2007 – 2017 period. Calculated by LSQF from monthly*  
 443 *averages and medians.*

Species	Monthly	Annual slope	Unit	R, n, significance
GEM	average	7.69 ± 2.11	pg m <sup>-3</sup> yr <sup>-1</sup>	0.3098, 127, >99.9%
	median	7.01 ± 2.11		0.2846, 127, >99%
CO <sub>2</sub>	average	2.208 ± 0.018	ppm yr <sup>-1</sup>	0.9955, 132, >99.9%
	median	2.219 ± 0.017		0.9964, 132, >99.9%
Rn	average	-0.76 ± 7.96	mBq m <sup>-3</sup> yr <sup>-1</sup>	-0.0085, 130, ns
	median	0.05 ± 4.58		0.0009, 130, ns
CO	average	-1.020 ± 0.301	ppb yr <sup>-1</sup>	-0.2848, 132, >99%
	median	-0.503 ± 0.223		-0.1939, 132, >95%
CH <sub>4</sub>	average	6.650 ± 0.402	ppb yr <sup>-1</sup>	0.8236, 132, >99.9%
	median	6.895 ± 0.335		0.8751, 132, >99.9%
O <sub>3</sub>	average	0.263 ± 0.151	ppb yr <sup>-1</sup>	0.1510, 131, ns
	median	0.260 ± 0.161		0.1408, 131, ns

444

445

446 Table 2: Trends at Amsterdam Island for the 2012 - 2017 period. *-Calculated by LSQF from*  
 447 *monthly averages and medians.*

Species	Monthly	Annual slope	Unit	R, n, significance
GEM	average	4.10 ± 3.65	pg m <sup>-3</sup> yr <sup>-1</sup>	0.1371, 68, ns
	median	5.57 ± 3.61		0.1865, 68, ns
CO <sub>2</sub>	average	2.487 ± 0.025	ppm yr <sup>-1</sup>	0.9962, 72, >99.9%
	median	2.487 ± 0.026		0.9959, 72, >99.9%
Rn	average	-1.626 ± 1.018	mBq m <sup>-3</sup> yr <sup>-1</sup>	-0.190, 70, ns
	median	-0.557 ± 0.604		-0.111, 70, ns
CO	average	-1.530 ± 2.405	ppb yr <sup>-1</sup>	-0.131, 25, ns
	median	-1.460 ± 2.351		-0.128, 25, ns
CH <sub>4</sub>	average	8.575 ± 0.786	ppb yr <sup>-1</sup>	0.7932, 72, >99.9%
	median	8.555 ± 0.793		0.7899, 72, >99.9%

448

449 Table 3. Trends at Cape Point for the 2012 – 2017 period. *Calculated by LSQF from monthly*  
 450 *averages and medians.*

Species	Monthly	Annual slope	Unit	R, n, significance
GEM	average	-8.65 ± 4.63	pg m <sup>-3</sup> yr <sup>-1</sup>	-0.2211, 70, ns
	median	-9.31 ± 4.55		-0.2409, 70, >95%
CO <sub>2</sub>	average	2.459 ± 0.035	ppm yr <sup>-1</sup>	0.9931, 72, >99.9%
	median	2.466 ± 0.030		0.9949, 72, >99.9%
Rn	average	20.05 ± 18.87	mBq m <sup>-3</sup> yr <sup>-1</sup>	0.1269, 71, ns
	median	15.36 ± 10.51		0.1732, 71, ns
CO	average	-0.151 ± 0.692	ppb yr <sup>-1</sup>	-0.0260, 72, ns
	median	0.053 ± 0.540		0.0117, 72, ns
CH <sub>4</sub>	average	9.160 ± 0.979	ppb yr <sup>-1</sup>	0.7455, 72, >99.9%
	median	9.498 ± 0.818		0.8111, 72, >99.9%

451

452



453 Table 4: Correlation of 3 months running average and median GEM concentrations and CO  
 454 mixing ratios with 3 months running average of SOI  
 455 ([www.cpc.ncep.noaa.gov/data/indices/soi.3m.txt](http://www.cpc.ncep.noaa.gov/data/indices/soi.3m.txt)). The CPT GEM data for 2007 – 2014 were  
 456 detrended, the CPT CO data for 2007-2014 and 2012-2017 deseasonalized using the average  
 457 monthly averages or medians over the period. No CO correlation is presented for AMS  
 458 because CO data are available only since December 2015 until December 2017. The delay  
 459 given in the last column is the one with the highest R. The delays in the brackets are  
 460 significant correlations with the second and third highest R.

Feldfunktion geändert

461

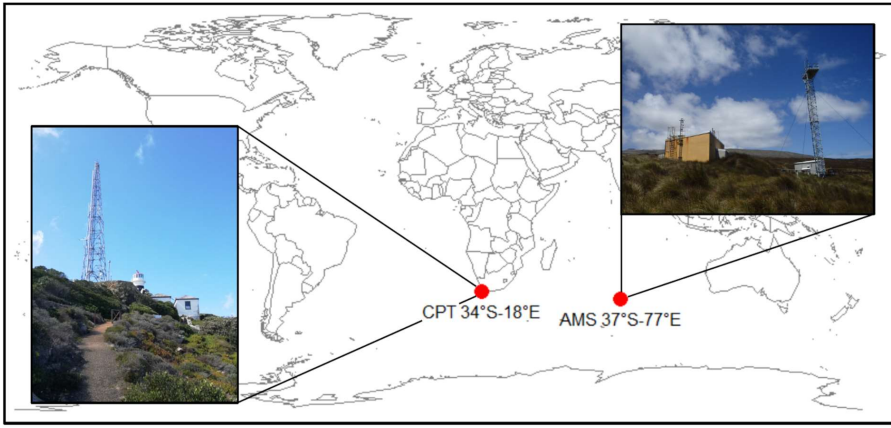
Site and period		Equation	R, n, signif.	GEM delay [month]
AMS, GEM, 2012–2017	average	$GEM = -0.0227 * SOI + 1.0375$	-0.4145, 70, >99.9%	7 (6-8)
	median	$GEM = -0.0230 * SOI + 1.0390$	-0.4150, 70, >99.9%	7 (6-8)
CPT, GEM, 2007-2014	average	$relGEM = -0.0330 * SOI + 1.0179$	-0.4554, 95, >99.9%	10 (9-11)
	median	$relGEM = -0.0373 * SOI + 1.0202$	-0.4934, 95, >99%	10 (9-11)
CPT, CO, 2007-2014	average	$relCO = -0.0367 * SOI + 1.0199$	-0.4171, 95, >99.9%	10 (9-11)
	median	$relCO = -0.0340 * SOI + 1.0184$	-0.5406, 95, >99.9%	10 (9-11)
CPT, GEM, 2012-2017	average	$GEM = 0.0318 * SOI + 1.0371$	0.4523, 69, >99.9%	8 (7-9)
	median	$GEM = 0.0279 * SOI + 1.0385$	0.3906, 69, >99.9%	7 (7-9)
CPT, CO, 2012-2017	average	$relCO = 0.0173 * SOI + 0.9995$	0.2358, 71, >95%	8 (9)
	median	$relCO = 0.0196 * SOI + 0.9991$	0.2914, 71, >95%	9 (10-11)

462

463

464 **Figures**

465



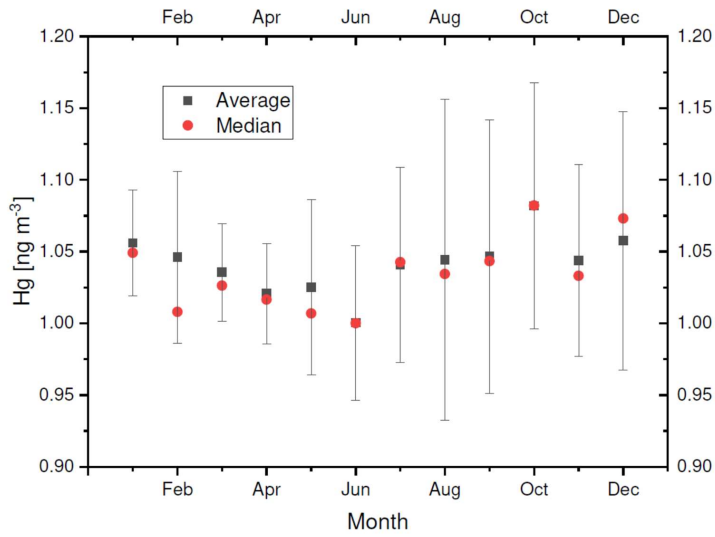
466

467

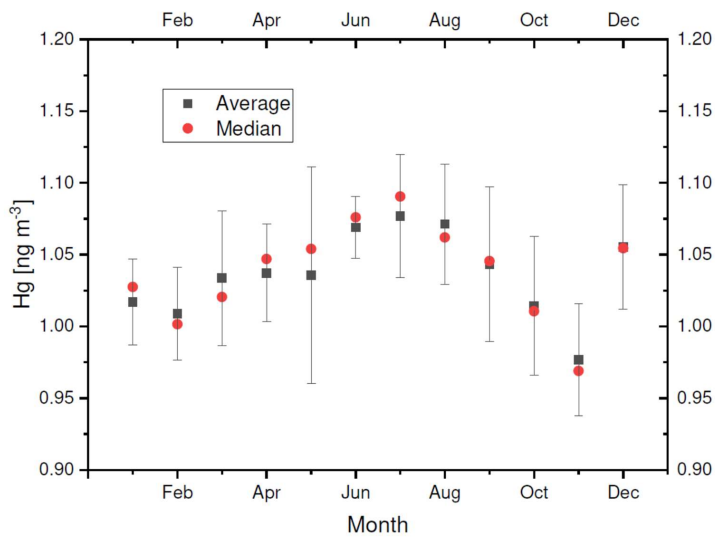
468 Figure 1: Location of the Cape Point (CPT) and Amsterdam Island (AMS) stations.

469

470



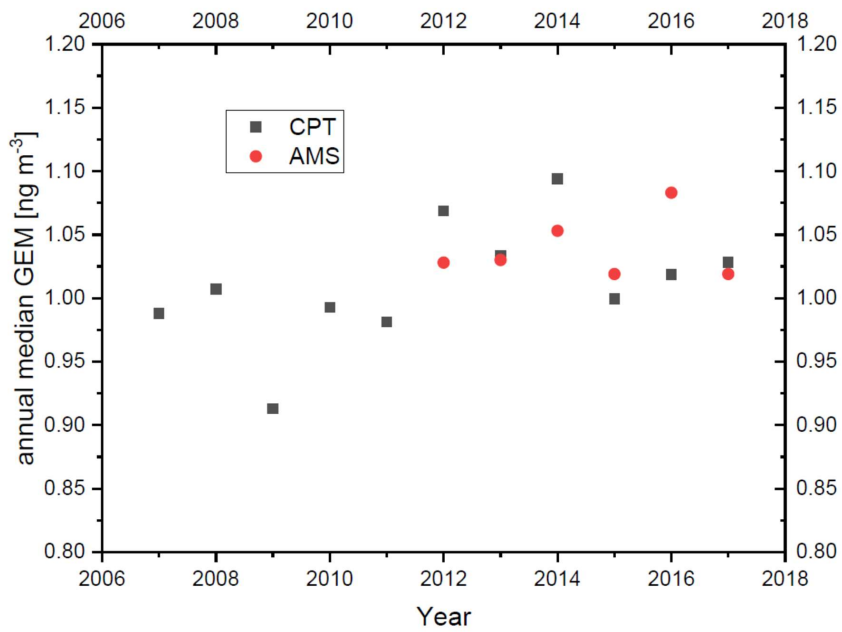
471



472

473 Figure 24: Seasonal variation of GEM in 2012 – 2017 at CPT (upper panel) and AMS (lower  
 474 panel). The points represent averages and medians of monthly medians over the 2012 – 2017  
 475 period. The bars represent the standard deviations of the monthly averages.

476



477

478

479 Figure 32: Annual median GEM concentrations at Cape Point (CPT) since March 2007 until  
 480 December 2017 and at Amsterdam Island (AMS) since February 2012 until December 2017.

481